AGU PUBLICATIONS

JGR

Journal of Geophysical Research: Solid Earth

RESEARCH ARTICLE
10.1002/2014JB011480

Key Points:
- Structure and stress patterns in Rotokawa display heterogeneity
- Structural heterogeneity patterns are typical of normal faulting
- Stress field orientation heterogeneity due to slip on fracture planes

Correspondence to:
D. D. McNamara,
d.mcnamara@gns.cri.nz

Citation:
McNamara, D. D., C. Massiot, B. Lewis, and I. C. Wallis (2015), Heterogeneity of structure and stress in the Rotokawa Geothermal Field, New Zealand, *J. Geophys. Res. Solid Earth*, *120*, doi:10.1002/2014JB011480.

Received 23 JUL 2014
Accepted 23 NOV 2014
Accepted article online 4 DEC 2014

Heterogeneity of structure and stress in the Rotokawa Geothermal Field, New Zealand

David D. McNamara[1], Cécile Massiot[2], Brandon Lewis[3], and Irene C. Wallis[4]

[1]GNS Science, Lower Hutt, New Zealand, [2]School of Geography, Environment and Earth Sciences, Victoria University of Wellington, Wellington, New Zealand, [3]GNS Science, Wairakei Research Centre, Taupo, New Zealand, [4]Mighty River Power Ltd., Rotorua, New Zealand

Abstract Geometric characterization of a geothermal reservoir's structures, and their relation to stress field orientation, is vital for resource development. Subsurface structure and stress field orientations of the Rotokawa Geothermal Field, New Zealand, have been studied, for the first time, using observations obtained from analysis of three acoustic borehole televiewer logs. While an overall NE-SW fracture strike exists, heterogeneity in fracture dip orientation is evident. Dominant dip direction changes from well to well due to proximity to variously oriented, graben-bounding faults. Fracture orientation heterogeneity also occurs within individual wells, where fractures clusters within certain depth intervals have antithetic dip directions to the well's dominant fracture dip direction. These patterns are consistent with expected antithetic faulting in extensional environments. A general S_{Hmax} orientation of NE-SW is determined from induced features on borehole walls. However, numerous localized azimuthal variations from this trend are evident, constituting stress field orientation heterogeneity. These variations are attributed to slip on fracture planes evidenced by changes in the azimuth of drilling-induced tensile fractures either side of a natural fracture. Correlation of observed fracture properties and patterns to well permeability indicators reveal that fractures play a role in fluid flow in the Rotokawa geothermal reservoir. Permeable zones commonly contain wide aperture fractures and high fracture densities which have a dominant NE-SW strike orientation and NW dip direction. Studies of this kind, which show strong interdependency of structure and stress field properties, are essential to understand fluid flow in geothermal reservoirs where structural permeability dominates.

1. Introduction

Recent years have seen an increased interest in accessing and utilizing natural and enhanced geothermal resources [*Bertani*, 2012]. Such resources are often hosted within crystalline, volcanic and plutonic reservoir rocks, in indurated, metamorphic basement reservoirs, and in sedimentary deposits [*Wood et al*., 2001; *Asanuma et al*., 2005; *Legarth et al*., 2005; *Sausse et al*., 2006; *Blackwell et al*., 2007]. Successful development of these reservoirs is dependent on understanding permeability, and in the case of the aforementioned geothermal resources, that permeability is dominantly secondary (faults and fractures), with only small contributions made by primary permeability [*Brace*, 1980; *Davatzes and Hickman*, 2010a; *Dezayes et al*., 2010]. As such, structural information, including spatial distribution, orientation, aperture, and fracture fill, is vital to the development of any geothermal reservoir hosted in igneous or metamorphic rocks.

Wide aperture fractures and high fracture densities commonly correlate to permeable zones in geothermal wells [*Barton et al*., 1998; *Sheridan and Hickman*, 2004; *McLean and McNamara*, 2011; *Wallis et al*., 2012; *Co*, 2012]. Fracture length and connectivity, their interrelationship, and the relationship between these factors and fracture aperture and density are also important when considering structural permeability in geothermal reservoirs [*Long and Witherspoon*, 1985; *Lee et al*., 2011; *Barton et al*., 2013]. Increased connectivity and density of a fracture network in a reservoir will often allow for higher permeability associated with the presence of longer fractures (in turn associated with wider apertures) [*Long and Witherspoon*, 1985; *Gudmundsson et al*., 2002; *Philipp et al*., 2013]. In addition, the relationship between structural patterns and in situ stress field orientations is important when considering permeability in geothermal reservoirs. Studies show that fractures optimally oriented within the current stress field can be subject to cyclical slip thus acting as open, fluid flow pathways [*Barton et al*., 1998; *Ito and Zoback*, 2000; *Sausse et al*., 2006; *Yoshioka and Stimac*, 2010; *Davatzes and Hickman*, 2010b].

Where stress orientation does play a significant role in determining a structure's fluid conductivity, understanding in situ stress field perturbations and their causes becomes important. At the geothermal field scale of investigation (tens of kilometers), heterogeneity in in situ stress field orientation can result from topography [*Zhang and Stephansson*, 2010], intrusion of magmatic rocks [*Johnson*, 1961; *Vigneresse et al*., 1999], intrinsic mechanical anisotropy within or between lithologies [*Bruno and Winterstein*, 1994; *Wileveau et al*., 2007], and, most commonly, slip on geological structures [*Martin and Chandler*, 1993; *Valley and Evans*, 2010; *Lin et al*., 2010; *Davatzes and Hickman*, 2010a; *Blake*, 2013; *Nie et al*., 2013]. In addition, field operations (i.e., production and injection) can directly cause stress orientation perturbations (e.g., through significant changes in reservoir pore pressure) or indirectly by inducing slip on reservoir structures [*Zhang and Stephansson*, 2010; *Blake and Davatzes*, 2011; *Sewell et al*., 2013].

Geothermal resources in the Taupo Volcanic Zone (TVZ), New Zealand, are often hosted in lithologies with low primary permeability such as volcanics (andesites and rhyolites, $9.95\times10^{-9}-1.68\times10^{-7}$ md), welded and indurated ignimbrites and tuffs, pervasively silicified volcaniclastic deposits, and greywacke basement rocks (4.89×10^{-7} md) [*Rowland and Sibson*, 2004; *Rosenberg et al*., 2009; *Bignall et al*., 2010; *Milicich et al*., 2013; *Siratovich et al*., 2014; *McNamara et al*., 2014]. Structure and stress characterization in these reservoirs is increasingly employed to assess and optimize resource utilization; however, this characterization is hindered by a lack of surface exposure, few drill cores, difficulty with geophysical imaging (e.g., seismic reflection) of the subsurface, and operational challenges and technological constraints on traditional logging technology.

This paper aims to provide the first characterization of and discussion of the relationship between fracturing and in situ stress orientation patterns within the Rotokawa Geothermal Field subsurface, using data acquired with a high-temperature borehole televiewer (BHTV). In addition, these borehole data have been examined in conjunction with available field-scale observations of faulting, lithological and structural information from drill cuttings and core, well completion test data (pressure, temperature, and fluid velocity), and fault patterns inferred from 3-D geological visualization of the field. This combined investigation provides an insight into structure and stress orientation patterns across this geothermal field, and the role of fracturing and stress in fluid flow in this geothermal reservoir.

2. Geological Setting

The Rotokawa Geothermal Field occupies an area ~28 km^2, located ~10 km northeast of Taupo in the central TVZ (Figure 1) [*Bibby et al*., 1995; *Risk*, 2000]. The TVZ represents the active part of the Central Volcanic Region, an extensional intra-arc basin formed as a result of subduction of the Pacific Plate beneath the North Island of New Zealand [*Wilson et al*., 1995; *Cole and Spinks*, 2009; *Begg and Mouslopoulou*, 2010; *Alcaraz et al*., 2011; *Rowland and Simmons*, 2012]. Extension in the TVZ is accommodated by the Taupo Rift, a series of dominantly NE-SW striking, normal faults with a vertical maximum principal stress ($\sigma_1 = S_v$) and a NW-SE extension/minimum horizontal stress direction ($\sigma_3 = S_{hmin}$) [*Hurst et al*., 2002; *Nicol et al*., 2006; *Hurst et al*., 2008; *Townend et al*., 2012]. Rifting commenced 1–2 Ma and continues to the present day with extension rates decreasing from ~15 mm/yr at the coast of Bay of Plenty to ~3 mm/yr at the rift termination (south of Lake Taupo) [*Wilson et al*., 1995; *Villamor and Berryman*, 2001; *Wallace et al*., 2004; *Begg and Mouslopoulou*, 2010].

The geology of the field has been detailed in previous works [*Grindley et al*., 1985; *Collar and Browne*, 1985; *Krupp and Seward*, 1987; *Browne et al*., 1992; *Arehart et al*., 2002; *Rae*, 2007; *Rae et al*., 2011]. The basement is composed of Late Palaeozoic to Late Mesozoic greywacke and argillite rocks of the Torlesse Supergroup. Overlying the basement is a laterally extensive, thick sequence of andesites (0.9–1.9 Ma) which is likely comprised of several flows [*Arehart et al*., 2002]. Above the andesite sequence lie the volcaniclastic and sedimentary deposits of the Reporoa Group (Tahorakuri and Waikora Formations) and, in places, the stratigraphically younger Wairakei Ignimbrite. These are overlain by rhyolite lavas and domes, the volcano-sedimentary Waiora Formation, and the sedimentary Huka Falls Formation. Hydrothermal eruption breccias and tephras cover the surface of the geothermal field.

Active, NE-SW striking, fault traces are present at the surface in the northwest of the field (Aratiatia Fault Zone), and a NE-SW alignment of hydrothermal eruption vents (including Lake Rotokawa) crosscuts the southern portion of the field [*Collar and Browne*, 1985; *Krupp and Seward*, 1987; *Rae*, 2007] (Figure 1). Mapping and photogeological studies [*Collar and Browne*, 1985; *Krupp and Seward*, 1987] display NE-SW striking, normal faults that displace the Oruanui Formation in the center of the field and to the north of Lake Rotokawa. Geological

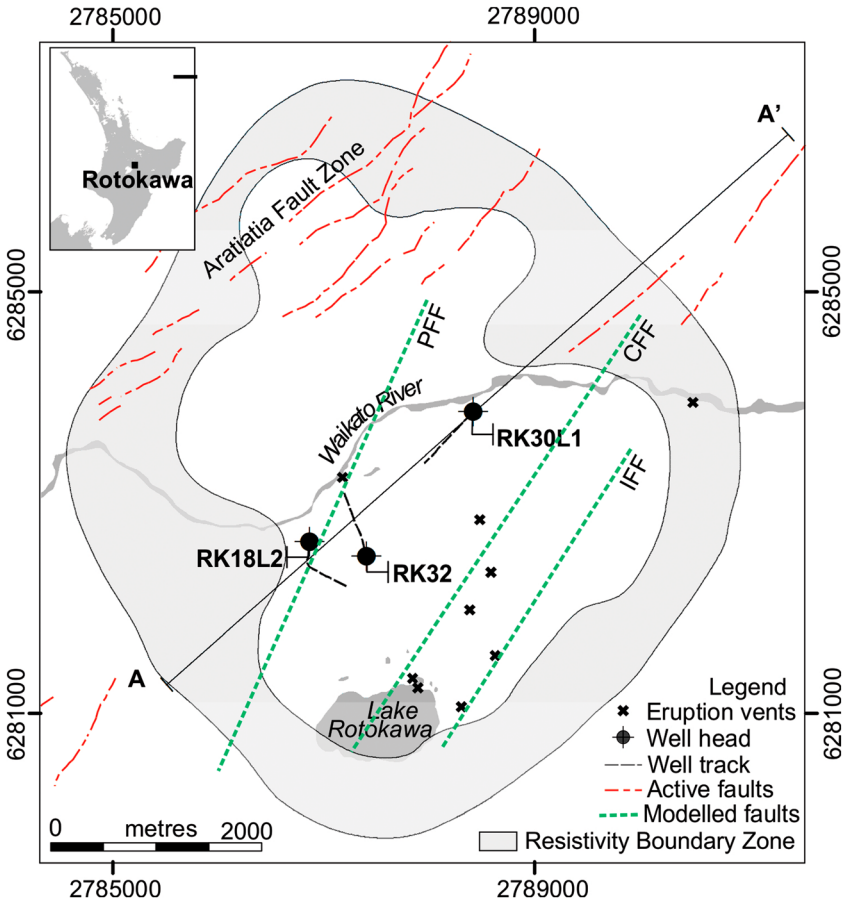

Figure 1. Location map of the Rotokawa Geothermal Field showing active faults [*Litchfield et al.*, 2014], locations of eruption vents, the three study wells and their well tracks, and the field resistivity boundary [*Risk*, 2000]. Inset shows location of the field on the North Island, New Zealand. Line A-A' is the line of cross section for Figure 2.

data from drilling (including observations of repeated stratigraphic units) and 3-D modeling of the field imply a NE-SW trending graben present at depth [*Grindley et al.*, 1985; *Collar and Browne*, 1985; *Krupp and Seward*, 1987; *Rae*, 2007; *Wallis et al.*, 2013]. This graben is bound to the NW by the SE dipping Injection Field Fault (IFF) and to the SE by the NW dipping Central Field Fault (CFF) and Production Field Fault (PFF). In addition, a paleovalley structure is inferred to be present in the top surface of the andesites, though the exact geometry of this feature is poorly constrained. The PFF, CFF, and IFF are continuous through the greywacke basement, andesites, and other units older than the Wairakei Ignimbrite [*Wallis et al.*, 2013]. At the top of this Wairakei Ignimbrite, which lies at around 1400 mVD (vertical meters), elevation differences in geologic units correlated between wells only suggest small, if any, reactivation of the PFF, CFF, and IFF. Microearthquake data further define the NE-SW striking CFF and suggests that it acts as a barrier to fluid flow across strike but is permeable along strike, consistent with tracer test observations [*Sewell et al.*, 2013].

The geothermal field can be vertically divided into three reservoirs separated by impermeable formations: a deep, hot, convecting, geothermal reservoir, an intermediate level aquifer and a shallow, hydrothermally altered aquifer [*Sewell et al.*, 2012]. Structure is the predominant control on fluid flow in the productive reservoir, which is mainly hosted in andesite, and larger, kilometer-scale faults are thought to compartmentalize this reservoir [*Rae*, 2007; *Heise et al.*, 2008; *Quinao and Sirad-Azwar*, 2012; *Quinao et al.*, 2013]. In the vicinity of the PFF, northeast fluid flow directions are determined from naphthalene sulfonate tracer tests [*Bannister et al.*, 2008]. *Sewell et al*. [2012] integrated MT models and natural state temperature interpretations to show a permeability decrease at the outer margin of the Rotokawa geothermal reservoir which was suggested to be the result of a decrease in the occurrence of open fractures. Permeability decreases to the west,

south, and east of the field are sharp (defined from strong lateral temperature gradients and well permeabilities) and are inferred to be fault controlled.

3. Methodology

BHTV logs were acquired over open-hole sections in three wells (RK18L2, RK30L1, and RK32) in the Rotokawa Geothermal Field using a high-temperature BHTV (Figure 1). This work presents the BHTV log analyses alongside the geology (including hydrothermal alteration) of these three wells, which is determined from examination of drill cuttings and core. In the absence of drill cuttings or core, geology is inferred from 3-D modeling and correlation to nearby wells [*Wallis et al*., 2013].

BHTV log acquisition was performed by Tiger Energy Services using the Acoustic Formation Imaging Technology tool, a high-temperature BHTV (rated to 300°C). Logs were acquired with a setting of 144 sample points per revolution and at a vertical logging speed of ~2–3 m/min, equivalent to an image resolution of ~5 mm vertically and ~10 mm horizontally.

BHTV logs were analyzed using Recall 5.4™ software and image features classified using the *Massiot et al*. [2015] system for TVZ geothermal acoustic image logs. Image quality is assessed qualitatively based upon visual assessment of the percentage of the image suitable for interpretation over 5 m intervals. Only continuous and discontinuous sinusoids (traced 360° and >275° around the borehole, respectively) are included in this data set. Partial sinusoids (traced <275° around the borehole) could only be observed with very low confidence and have been excluded. Systematic undersampling of features subparallel to the borehole axis has been corrected following *Massiot et al*. [2012]. Travel time data were used to calculate caliper values for the borehole which are calibrated for the variable speed of sound through water at the changing thermodynamic conditions of the borehole fluid [*Massiot et al*., 2015].

Fracture apertures were measured directly from the acoustic image and scaled to the average diameter of the borehole and, as such, are only approximations. Although apparent aperture can be proportional to the true aperture of a fracture, it does not directly correspond to the hydraulic aperture as many other physical properties can influence the acoustic impedance contrasts associated with a structure [*Cheung*, 1999; *Valley*, 2007; *Davatzes and Hickman*, 2010a]. Therefore, apparent aperture measurements presented here are most likely maximum estimates [*Davatzes and Hickman*, 2005] and are presented to provide insight into the relative importance of aperture variation.

Induced features (borehole breakouts, drilling-induced tensile fractures (DITF), and petal centreline fractures (PCFs)) observed on borehole acoustic images result from action of stress on the borehole walls and floor. In vertical to near-vertical wells, assuming that one of the principal stresses is vertical (S_v), the orientation of the in situ maximum horizontal stress direction (S_{Hmax}) can be determined from the orientation DITFs and the orientation of S_{hmin} from borehole breakout and petal centerline fracture orientations [*Zoback et al*., 2003; *Davatzes and Hickman*, 2005; *Schmitt et al*., 2012; *Massiot et al*., 2015]. For deviated wells (>15° from vertical), in a normal faulting environment (as expected in the TVZ), this relationship becomes more complicated and DITFs will form as en echelon pairs inclined to the wellbore axis [*Peška and Zoback*, 1995; *Aadnøy and Bell*, 1998; *Zoback*, 2010]. In addition, the preferential occurrence of induced features in geothermal wells is strongly influenced by temperature differences (ΔT) between the borehole fluid and the formation [*Brudy et al*., 1997; *Zoback et al*., 2003]. For the Rotokawa Geothermal Field, ΔT is typically >150°C at production depths and so the tensile stresses at the borehole wall are significantly increased due to rock contraction, making DITFs and PCFs more likely to form in response to stress around the borehole than borehole breakouts [*Davidson et al*., 2012].

The three study wells are deviated >15° from vertical (Table 1), and measurements of in situ horizontal stress orientations from induced features on these borehole walls must be corrected for that deviation angle. Such a correction requires knowledge of principal stress magnitudes and the mechanical properties of the rock type in which the induced feature is observed [*Peška and Zoback*, 1995]. Determination of these values in the Rotokawa Geothermal Field has been partially successful, with approximate values determined for S_v and S_{hmin} [*Davidson et al*., 2012]. The magnitude of the full stress tensor has not been confidently constrained because of the scarcity of appropriate measurements, complicated overburden stresses due to variable lithological thicknesses, and a complicated pressure gradient. The potential effect that well deviation may have on the in situ horizontal stress field orientations described here will be taken into account in the discussion.

Table 1. Borehole Trajectory Data of Study Wells Over BHTV Logged Intervals

	RK18L2	RK30L1	RK32
Well deviation range	16°–26°	20°–29°	17°–23°
Well azimuth range	086°–169°	212°–239°	303°–321°
Average well deviation	23° ± 2°	24° ± 1°	20° ± 1°
Average well azimuth	100° ± 16°	220° ± 4°	314° ± 3°

4. Results

4.1. Image Quality

Acoustic image quality in wells RK18L2, RK30L1, and RK32 is variable (Table 2). Degradation of acoustic image quality is dependent on a number of factors that affect the scattering of the acoustic wave (either at the borehole wall or in the well fluid) and prevent a signal returning to the BHTV. Causes of acoustic wave scattering include borehole rugosity, decentralization of the BHTV in the borehole, and the presence of image artefacts [*Lofts and Bourke*, 1999; *García-Carballido et al*., 2010]. As decentralization during logging was not an issue and there are few significant "stick and pull" image artefacts, neither is it responsible for noted areas of poorer image quality.

Calculated caliper values larger than the nominal borehole diameter (8.5 in./21.6 cm) are caused by intervals of poor borehole circularity, which correlate to image intervals with "very poor" to "poor" quality. Conversely, "moderate" to "good" image quality is mainly present over borehole intervals in which the calculated diameter is closer to the nominal borehole diameter, and the borehole shape is more cylindrical. Some intervals where calculated caliper values are close to the nominal borehole diameter display very poor and poor image quality. This is attributed to the effect of "spiral hole" and "stabilizer mark" image artefacts [*Lofts and Bourke*, 1999] which reduce the percentage of image available for interpretation. In some cases, large calculated caliper values are a result of enlargement around the full 360° of the borehole rather than poor circularity, and better quality image (moderate to good) is found. The majority of image degradation in the three study wells can be attributed to borehole rugosity due to drilling and logging processes (visualized as zones of data loss or image artefacts).

Comparison of image quality to lithology reveals that andesites are more likely than other volcaniclastic lithologies (mainly pyroclastics) to contain moderate to good image quality. This may be due to andesites being more mechanically stable during drilling resulting in a higher-quality drillhole (more cylindrical), thereby increasing the amount of acoustic signal returned from the borehole wall to the BHTV. A similar comparison of image quality to alteration intensity reveals no discernible pattern.

4.2. Feature Classification and Morphology

A total of 1775 natural features and 258 induced features were identified with high confidence on acoustic images from the three study wells (Table 3). All natural features are interpreted as fractures which have morphological relationships (as defined in *Massiot et al*. [2015]) that are *parallel* (46%, fractures with <1 m spacing with strike and dip orientation differences $<15°$ that do not crosscut on the BHTV log), *crosscutting* (25%, fractures that crosscut each other on the BHTV), and *solitary* (29%, neither parallel nor crosscutting). Fractures observed in wells RK18L2 and RK32 have dominantly parallel relationships (52% and 46%, respectively), and those in well RK30L1 have mainly parallel or crosscutting relationships (40% and 38%, respectively).

Table 2. Image Quality Percentages of Study Wells[a]

Well	Bad	Very Poor	Poor	Moderate	Good
RK18L2	0	20	46	34	0
RK30L1	1	25	46	28	0
RK32	4	8	37	36	15

[a]Image quality rankings: Bad (image cannot be used for interpretation), Very Poor (≤25% of image available for interpretation), Poor (>25% but ≤50% of image available for interpretation), Moderate (>50% but ≤75% of image available for interpretation), and Good (>75% of image available for interpretation).

Table 3. Number of Features Observed on BHTV Logs of Study Wells[a]

	RK18L2	RK30L1	RK32	Total
		Fractures		
Low-amplitude fracture	164 (S), 276 (P), 93 (CC) = 533 (T)	139 (S), 248 (P), 240 (CC) = 627 (T)	214 (S), 284 (P), 116 (CC) = 614 (T)	1774
High-amplitude fracture	0	1 (P)	0	1
		Induced Features		
DITF	26	87	27	140
SDITF	26	30	21	77
Borehole breakout	0	0	1	1
PCF	12	13	15	40

[a](S) = Solitary fracture relationship, (P) = Parallel fracture relationship, (CC) = Crosscutting fracture relationship, and (T) = Total number of fractures in individual well.

Induced features include DITFs, single DITFs (SDITFs), borehole breakouts, and petal centerline fractures (PCFs). Single DITFs are identified as one of a pair of DITFs, the other of which is obscured by poor image quality in its expected, corresponding azimuth on the borehole wall. They are treated as low confidence-induced features. DITFs and SDITFs are more numerous than borehole breakouts and PCFs in the imaged Rotokawa wells. DITFs display morphologies axial to the borehole; no en echelon DITF types are observed with confidence. In addition, ~75% of DITFs were observed to terminate against fracture planes, while the remaining 25% were not in proximity to an observed structure, or poor image quality obscured any observable relationship.

4.3. Fracture Orientation

Fracture orientation measurements, using data sets corrected for well orientation bias, show 69% of all fractures dip steeply at ≥70°. Individual wells display similar proportions of steeply dipping fractures; 81%, 60%, and 66% of fractures dip ≥70° in RK18L2, RK30L1, and RK32, respectively. Fractures dominantly dip SE and NW (Table 4). These dominant fracture dip directions vary between and within wells, i.e., wells RK18L2 and RK30L1 have dominantly SE (38%) and NW (34%) dips, respectively, while the fractures in well RK32 have a bimodal, dominant dip direction distribution (38% dipping SE and 29% dipping NW). These steeply dipping, NE-SW striking fractures have mainly parallel morphological relationships with other nearby fractures.

Vector azimuth plots of fracture dip directions for each of the wells reveals variation of fracture orientation with depth (Figure 2). Although wells RK18L2 and RK30L1 show dominant dip directions of SE and NW, respectively, they contain intervals in which fractures with dip directions either opposite to the dominant direction or have no dominant direction (variable orientation). The bimodality of fracture dip directions in well RK32 is not ubiquitous along the well; rather, it displays alternating zones of NW or SE dominated dip directions, with only two identifiable depth intervals with approximately equal proportions of NW and SE dipping fractures (bimodal).

4.4. Fracture Density

Fracture density in the three study wells is variable (Figure 3). Peaks in fracture density are identified here as any 10 m depth interval that has >10 fractures. Wells RK18L2, RK30L1, and RK32 have 18, 15, and 16 intervals

Table 4. Fracture Dip Azimuths (%) for Total Well and Individual Well Data Sets[a]

Dip Direction	Total Well Fractures	RK18L2 Fractures	RK30L1 Fractures	RK32 Fractures
N	5%	3%	7%	5%
NE	3%	5%	2%	1%
E	14%	25%	8%	9%
SE	28%	38%	12%	38%
S	9%	8%	11%	6%
SW	6%	6%	8%	2%
W	12%	7%	19%	9%
NW	23%	7%	34%	29%

[a]N = 337.5°–022.5°, NE = 022.5°–067.5°, E = 067.5°–112.5°, SE = 112.5°–157.5°, S = 157.5°–202.5°, SW = 202.5°–247.5°, W = 247.5°–292.5°, and NW = 292.5°–337.5°.

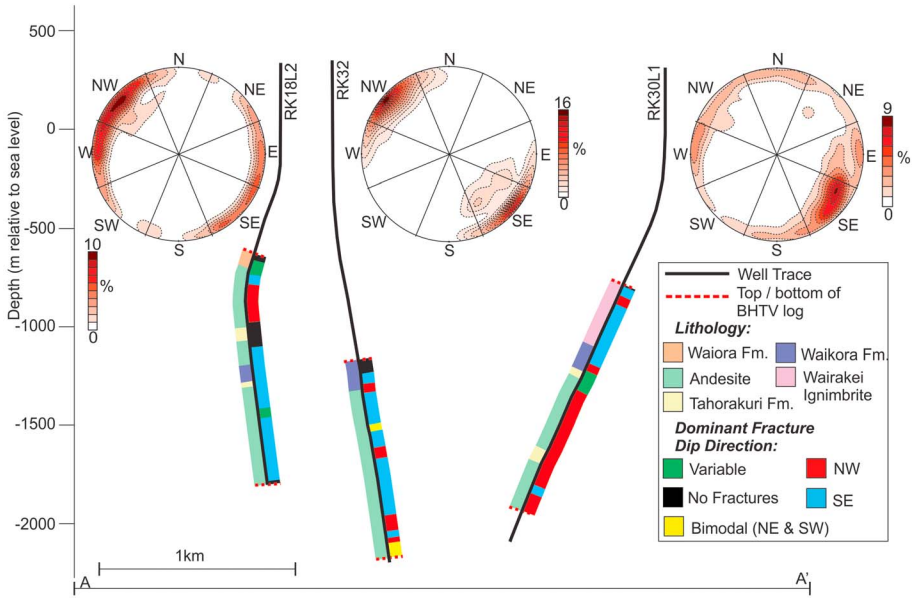

Figure 2. Cross section (Line A-A′ in Figure 1) with projected RK18L2, RK30L1, and RK32 well tracks. Left side of well traces colored for lithology (determined from drill cuttings/core and geological modeling) and right side colored for dominant fracture dip direction (as determined from vector azimuth plots). Contoured, lower hemisphere stereonets of poles to planes show fracture orientation pattern for each well. Stereonets contoured using Fisher Distribution with color scales representing percentages [*Grohmann and Campanha*, 2010]. Fm. = Formation.

of >10 fractures/10 m, respectively, representing ~11% of the imaged portions of the study wells. Most high fracture densities occur in andesite, with only one occurring in the lower Tahorakuri Formation of well RK18L2. High fracture densities within andesite mainly occur within the unit except for well RK30L1 where high fracture densities are noted at the top of both andesite units. Fractures in high-density intervals display mainly parallel morphological relationships.

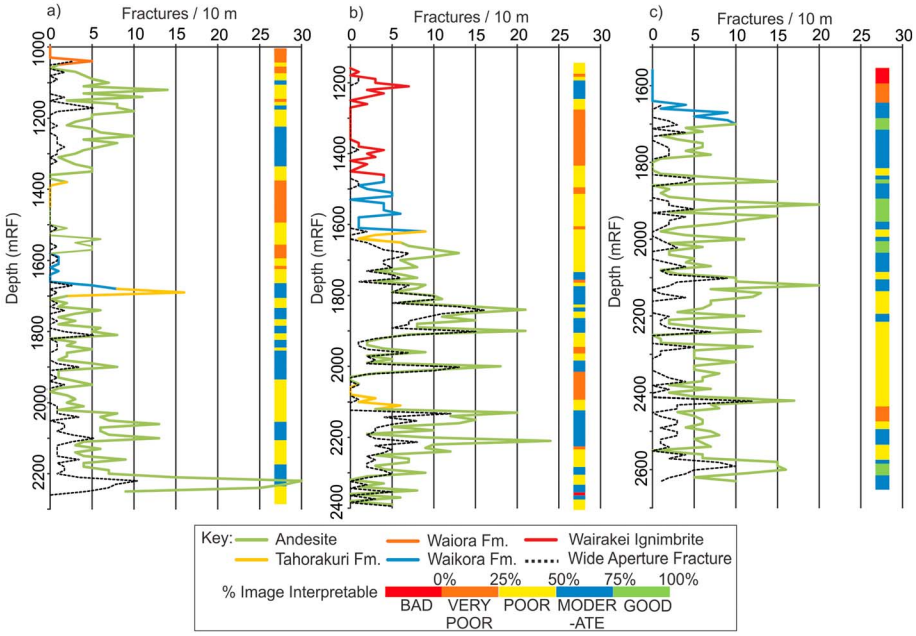

Figure 3. Fracture density plots for wells (a) RK18L2, (b) RK30L1, and (c) RK32. Fracture density curve colored by lithology. Black dashed line represents frequency of wide aperture fractures. Image quality represented by colored bar on the right side of each plot.

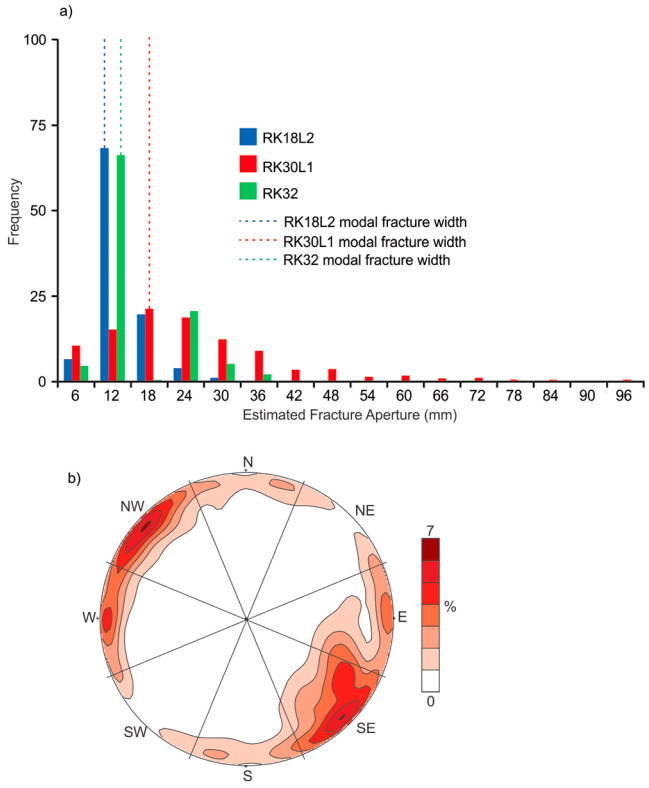

Figure 4. (a) Frequency plot of fracture widths for each study well. (b) Lower hemisphere, contoured stereonet of poles to planes of wide aperture fractures. Stereonets contoured using Fisher Distribution with color scales representing percentages.

Fracture density is compared against image quality to determine bias (Figure 3). In all three study wells, high fracture densities are predominantly found in intervals of moderate or good image quality. Low fracture densities are commonly observed in image intervals of very poor and poor quality. Comparison of fracture density between intervals of high and low image quality is not possible as geological and induced features are likely less visible in low image quality intervals. Despite this, observed fracture density variation in image intervals of better image quality is at least partially natural, as both high and low fracture densities are observed within these intervals.

4.5. Fracture Width

Wide fractures are defined as those with estimated apertures greater than the modal aperture for a given well (Figure 4a). Narrow aperture fractures (with widths below the modal aperture for a given well) dominate (~70%) the total fracture population in all wells (Figure 4a). Approximately 41% of wide aperture fractures are located in well RK30L1. In addition, 96% of wide aperture fractures are located within andesite (Figure 3). Approximately 30% of wide aperture fractures occur in intervals of high fracture density (Figure 3), and 50% have SE or NW dip directions (Figure 4b). Wide aperture fractures have variable morphological relationships to other fractures (i.e., parallel, crosscutting, and solitary).

4.6. In Situ Horizontal Stress Field Orientation

The weighted average orientations and standard deviations (uncorrected for well deviation; for further note see section 5) of the in situ horizontal stress field orientations are shown in Figure 5 and listed in Table 5. Well RK18L2 shows a depth-related, bimodal S_{Hmax} orientation with ENE-WSW orientations over the interval ~1170–1390 mRF (meters to rig floor), and NE-SW orientations over the interval ~1510–2160 mRF (Figure 5d). Wells RK30L1 and RK32 show S_{Hmax} orientations of NNE-SSW and S_{hmin} orientations of ESE-WNW.

S_{Hmax} orientation measurements from all three study wells display localized variations highlighting rotations in the in situ horizontal stress field orientation. Numerous rotations of $\leq$30° in S_{Hmax} orientation occur within 10 m depth intervals (Table 5). The largest rotations in S_{Hmax} orientation over localized depth intervals occur in well RK32: ~1690–1710 mRF (between 019°and 059°) and ~2045–2100 mRF (between 013° and 051°, Figure 5f).

5. Discussion

Results from BHTV log analyses indicate that over the western Rotokawa Geothermal Field, fracture and in situ horizontal stress field orientations are heterogeneous. This heterogeneity exists on various scales, both between and within wells. Such variation has important consequences for understanding the evolution of the field geology and structure, fluid flow, and reservoir behavior.

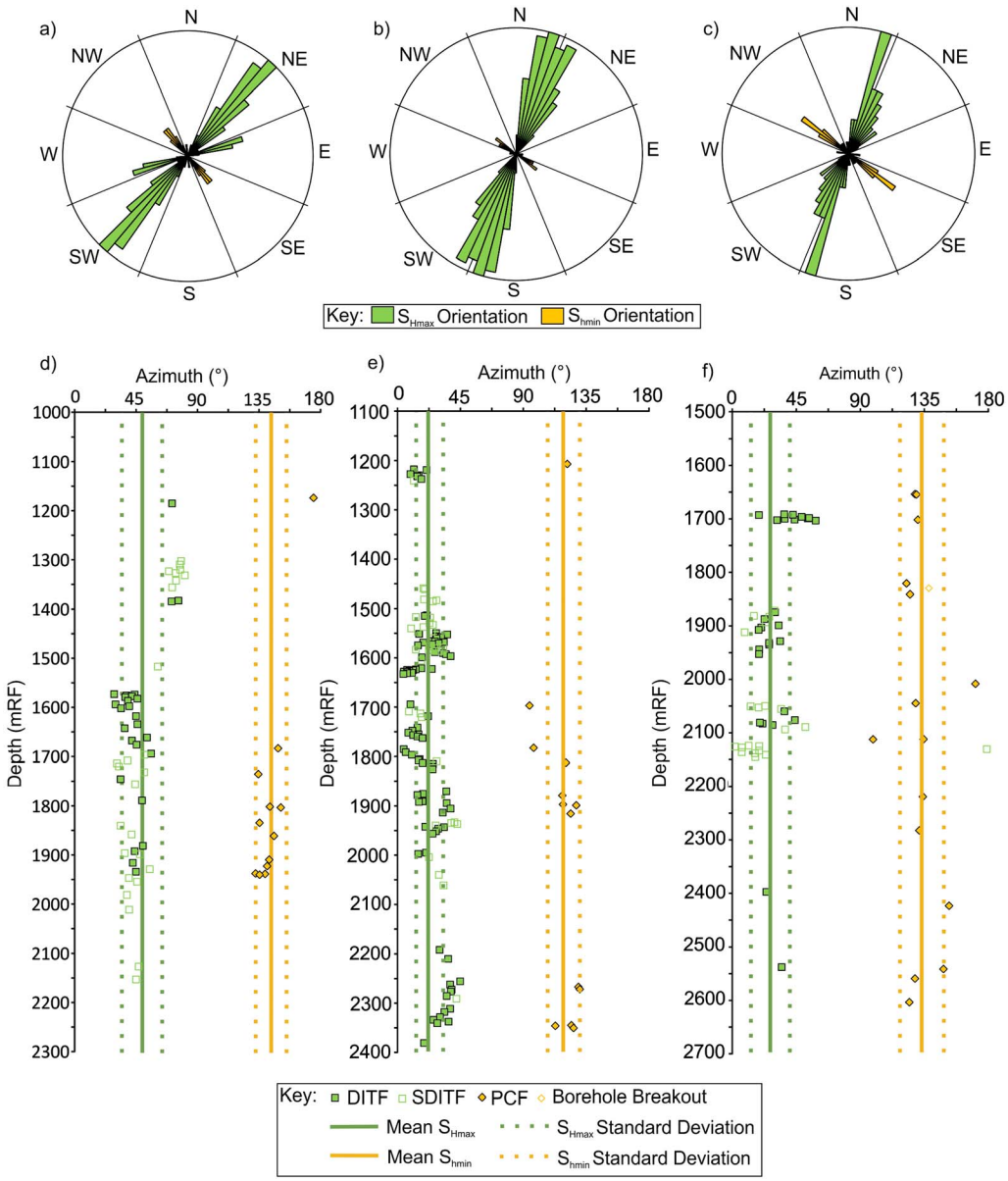

Figure 5. Bidirectional rose diagrams showing in situ horizontal stress orientations for wells (a) RK18L2, (b) RK30L1, and (c) RK32. Depth plots of in situ horizontal stress orientations for wells (d) RK18L2, (e) RK30L1, and (f) RK32.

5.1. Nature of Observed Structures

Critical to the structural characterization of a reservoir, and understanding a structures potential for permeability, is knowing whether structures are open or filled and whether they are tectonic or result from other processes such as cooling jointing in a volcanic unit or opening of planes of weakness at the borehole

Table 5. S_{Hmax} Orientation Measurements Weighted by Length of Measured DITF

	RK18L2	RK30L1	RK32
Mean	049°	025°	030°
Standard deviation	±15°	±11°	±23°
Range	029°–081°	004°–045°	359°–059°
Maximum variation in S_{Hmax} over any given 10 m interval	15°	21°	30°

wall caused by drilling. Detection of any geological feature using a BHTV requires an acoustic contrast between the feature and the host lithology. Studies in hydrocarbon and geothermal wells [*Parkinson et al*., 1999; *Davatzes and Hickman*, 2010b] imply that low acoustic amplitude fractures are either (a) open, (b) filled with drilling muds, (c) filled with clay/mud derived from the borehole wall lithology, (d) filled with hydrothermal minerals (e.g., hydrothermal clays (illite/smectite), iron oxides), or (e) any combination of these. In contrast, those fractures with high acoustic amplitude have been shown to be either mineral filled (e.g., quartz) or cataclastic planes.

Determining whether the low acoustic amplitude fractures observed in this study are open or closed relies on correlation with other sources of data (e.g., alteration logs, drill-cutting descriptions, and drill core). Imaged intervals of the three study wells were drilled with water ruling out low acoustic amplitude fractures filled with drilling mud. In addition, the imaged intervals of the wells were drilled through hard volcanic rock, containing evidence of fractures filled with epidote, quartz, chlorite, chalcedony, pyrite, hematite, and calcite, with little evidence of illite/smectite clay alteration (determined from drill cuttings and two drill cores). This rules out low acoustic amplitude fractures filled with clay/mud derived from the borehole wall. Thus, the low acoustic amplitude fractures observed in this study, which are the dominant type observed, are either open, partially open, or filled with hydrothermal minerals.

The common acoustic amplitude response of the mineral fills observed from drill cuttings and core, with the exception of quartz (high amplitude) and pyrite (low amplitude), has yet to be reported due to the scarcity of combined BHTV log and drill core data sets in geothermal environments. Chlorite, as a phyllosilicate, may have similar acoustic responses to those of illite/smectite and thus may be present in some of these low-amplitude fractures. The occurrence of only one high acoustic amplitude fracture suggests (a) that the low occurrence is a real phenomenon or (b) that the contrast between such features and the host lithologies is too small for them to be regularly resolved on the BHTV log; meaning, they are undersampled. Further study of the acoustic response of geothermal fracture fill mineralogy is required before it can be conclusively stated whether any of the low-amplitude fractures are open. This must be kept in mind when discussing the contribution of fractures to permeability.

Determining the origin of the fractures observed from BHTV logs is difficult. If the observed fractures are cooling joints in volcanic formations, certain fracture patterns should be present. The morphology of cooling joints in lava units varies depending on numerous factors such as the chemical composition and preexisting topography [*Hetényi et al*., 2012], the location within the flow and cooling rates [*DeGraff and Aydin*, 1987], and the interaction with glaciers [*Spörli and Rowland*, 2006]. Columnar-jointed lava flows usually contain units of entablatures (where columns are disordered), and colonnades (where columns are subparallel to each other) which can have pentagonal to hexagonal cross sections with variable strike orientations [*Budkewitsch and Robin*, 1994]. Rectangular cross sections of jointed andesite lava flows observed in the Tukino area, TVZ [*Spörli and Rowland*, 2006], a potential analogue to the andesite in the Rotokawa Geothermal Field, show two dominant fracture strike orientations related to the lava flow direction, formed independent of the local stress regime. It is thus possible, albeit rare, to have a dominant fracture orientation in colonnades.

Direct evidence of the tectonic nature of the fractures observed at depth in the Rotokawa Geothermal Field comes from drill core observations which show open and sealed fractures present in andesite. Slickensides on some fracture surfaces are evidence of slip alluding to tectonic action on these fractures, though it is noted here that slip is not a requirement for a fracture to be tectonic in origin. In addition, a drill core interval from well RK30L1 displays PCF development. This core was rotated, so the orientation of its PCF's matched the BHTV-derived S_{hmin} orientation over the same interval (Figure 6). This allowed assessment of core feature orientation which indicated a dominant NE-SW strike direction for observed natural fractures in the drill core, which is consistent with BHTV log observations.

Observation of a singular dominant fracture strike orientation (NE-SW) that is consistent with the regional trend of the rift, and observed evidence of tectonic action on some fracture planes, implies a tectonic origin for fractures observed on BHTV logs. There remains the possibility that these tectonic fractures are inherited from initial cooling joints. The BHTV log fracture population may represent those cooling joints optimally oriented for reactivation within the current stress field orientation. Cooling joints with different orientations may have become sealed, though there is little evidence for these orientations on BHTV logs or from the sparsely available drill core.

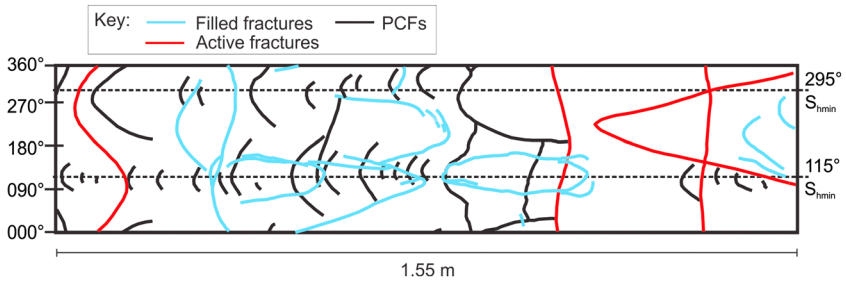

Figure 6. Image of fractures traced from RK30L1 andesite drill core oriented using acoustic image interpretation. The core shows fractures filled with hydrothermal minerals, active fractures, and PCFs.

5.2. Form and Origins of Structural Heterogeneity

The strike of fractures from the logged intervals in the three study wells show a NE-SW pattern which is parallel to the trend of the Taupo rift and the NE-SW strike of the main faults in the Rotokawa Geothermal Field and in nearby areas (e.g., the Aratiatia Fault Zone). The high dip angles recorded (>70°) are higher than expected from extensional tectonics (60°) [*Anderson*, 1905]. However, similar structural geometries (normal faults steeply dip (≥70°) at the surface and shallow (≥45°) toward seismogenic depths) are noted for faulting in other areas of the TVZ [*Villamor and Berryman*, 2001; *Lamarche et al*., 2006]. The direction of extension for this geological area is thought to have been consistently SE-NW for ~4 Ma [*Seebeck et al*., 2014], and so deposition of the Rotokawa volcano-sedimentary sequence (≥1.9 Ma) occurred within the same stress field recorded today. As such, all structures in these lithologies will have formed within this stress field orientation or as part of the depositional processes of these geological units.

While dominant trends in fracture orientation are present, variation is evident. Field-scale structural heterogeneity is apparent from changing dominant fracture dip directions between wells. Fracture orientations in the most northeastern well (RK30L1) display a dominant NW dip direction while the most southwestern well (RK18L2) exhibits mainly SE dip directions. Structural modeling of the geothermal field [*Wallis et al*., 2013] indicates that RK18L2 is located near the PFF, oriented 024°/89° SE, which defines the western side of a larger, NE-SW oriented, graben. The dominant fracture strikes (NE-SW) and steep SE dips in well RK18L2 are broadly consistent with this fault orientation.

Well RK30L1 is located within what is described as an ENE-WSW striking, potentially structurally bound, paleovalley; however, constraint of this existence of this paleovalley and any structure that may be a part of it is poor [*Wallis et al*., 2013]. Variations in the orientation of the in situ horizontal stress field orientations and repeated lithological sequences noted from drill cuttings and core may be evidence of faulting within the paleovalley. The dominant NW fracture dip direction observed may indicate a larger, NW dipping structure near well RK30L1, possibly antithetic to the PFF, although this interpretation is tenuous given the poorly constrained paleovalley and associated structures in this area of the geothermal field.

Well-scale variation from the dominant structural orientation (NE-SW) is observed in all three study wells. N-S fracture strike orientations are common, and rarer E-W and NW-SE strike orientations are also observed. These orientations have been noted in other areas of the TVZ [*McNamara et al*., 2013, and references therein] and thus can be expected as subordinate structural populations in the BHTV logged intervals of the Rotokawa Geothermal Field.

Vector azimuth plots of the fracture dip azimuth for wells RK18L2 and RK30L1 (Figure 2) show that there are depth intervals where fracture dip direction is antithetic to the dominant direction or has a set of fractures with variable dip directions. This phenomenon is particularly obvious in well RK32 where alternations between intervals of SE and NW dipping fractures are common, implying a complex structural arrangement in this area. In a normal faulting environment, localized populations of antithetic structures are expected, explaining the occasional changes between intervals of dominantly SE and NW dipping fractures. Well RK32 is located near the modeled PFF, intersecting it at ~2422 mRF. The frequent alternations in dominant dip direction may imply a number of NW dipping faults antithetic to the PFF. Well RK32 contains two intervals of variable fracture orientation. Two of these occur at the top of andesite intervals possibly representing a

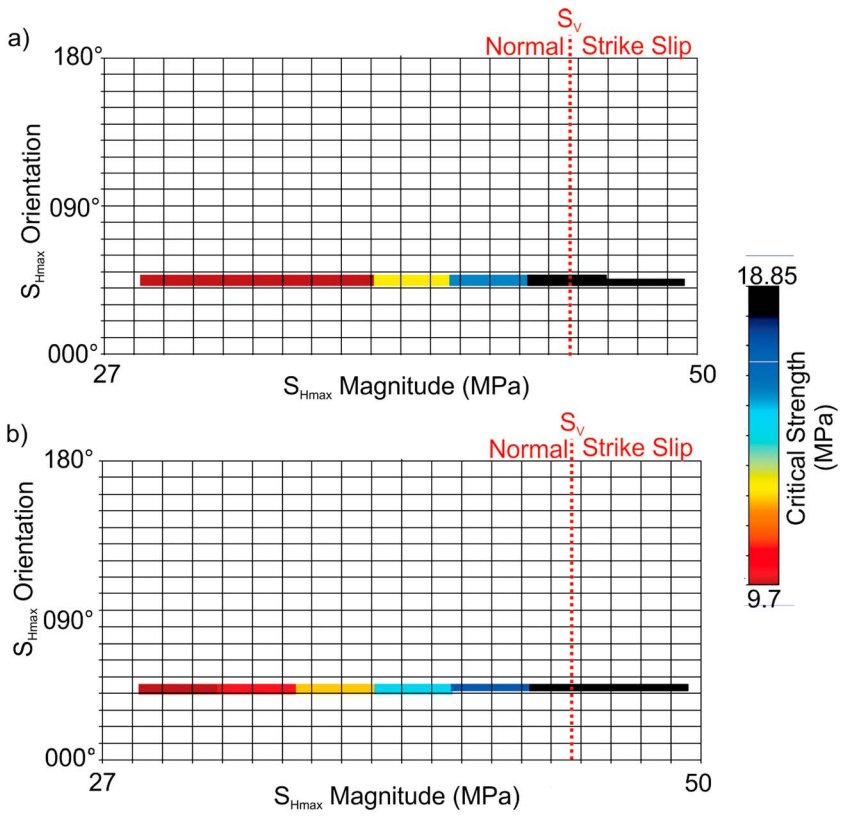

Figure 7. Plots of expected S_{Hmax} orientation for a range of S_{Hmax} magnitudes for well RK18L2 (~1955 mRF) when it is modeled as (a) a vertical well and (b) a well deviated 23° from vertical, trending 116°. Orientation range colored according to the critical strength of andesite (the tensile strength that needs to be exceeded to create a DITF). Conditions of model: S_v magnitude = 45 MPa, and S_{hmin} magnitude = 27 MPa.

rubbly, brecciated character common to lava flows. A third interval of variable fracture orientations occurs within an andesite interval in well RK18L2, again, possibly indicating a brecciated, rubble layer between two lava flows.

As fracture density is subject to image quality bias, comparison of fracture density between variable image qualities is not possible. For example, while andesite intervals appear to be more densely fractured than the volcaniclastics, this may be a signal of the image quality bias. As indicated earlier, andesites contain intervals of low and high fracture densities that do not appear to be related to image quality, implying natural variation. These high fracture density zones may represent intervals where the well passes through a fault zone, such as what occurs at ~2420 mRF in well RK32 (intersection of the PFF).

5.3. Confidence in Determined S_{Hmax} Orientation From DITFs

The deviation from vertical of the three study wells (Table 1) potentially introduces error into the determination of in situ horizontal stress field orientations from observation of induced features on a borehole surface. Numerous, measured S_{Hmax} azimuths from observed DITFs from the three study wells were modeled using the Petris Recall™ Sigma module for a range of given S_{Hmax} magnitudes ($S_{hmin} \leq S_{Hmax} \leq S_v$, values of S_{hmin} and S_v from *Davidson et al.* [2012]) for both the deviation of that well (at the observed depth of the DITF) and as if that well was vertical. For example, a DITF observed in RK18L2 at ~1955 mRF shows that for all S_{Hmax} magnitudes between S_v (45 MPa) and S_{hmim} (27 MPa), the orientation of S_{Hmax} in a vertical well and deviated well (23° from vertical, trending 116°) only varies by ~2° (Figure 7). This is within the margin of error attributed to measurement of induced features orientations from BHTV logs. Thus, despite deviation of the study wells, high confidence can be placed the in situ horizontal stress field orientations obtained from the BHTV logged intervals of the study wells.

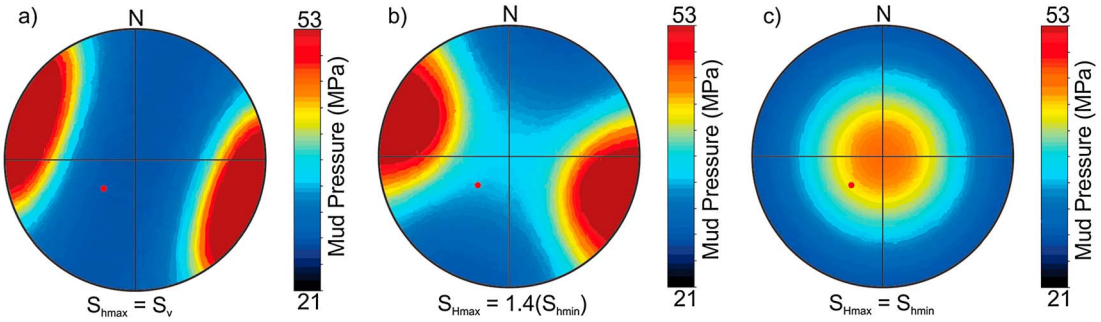

Figure 8. Stereograms showing the tendency for the initiation of DITFs to form in deviated well RK30L1 at ~2381 mRF (red dot) assuming (a) $S_{Hmax} = S_v$, (b) $S_{Hmax} = S_{hmin} + 40\%\ S_{hmin}$, and (c) $S_{Hmax} = S_{hmin}$. Color scheme represents mud pressures needed for DITF initiation (blue = low and red = high). Stereograms show well deviation angles of 0° (vertical) at the center to 90° (horizontal) at the rim. $T = 24$ MPa, $\Delta T = 100$°C, $S_v = 53$ MPa, $S_{hmin} = 32$ MPa, pore pressure (P_p) = 21 MPa, S_{Hmax} direction = 019°, well deviation = 25° from vertical, trending 225°.

5.4. Predominance of DITFs for In Situ Stress Orientation Measurements

It is known that borehole breakouts are less likely to develop in extensional environment than DITFs [*Zoback*, 2010]. However, it has been shown that in the Rotokawa Geothermal Field, ΔT is crucial to DITF formation [*Davidson et al*., 2012]. Numerous models were performed to observe the tendency of DITF initiation using the Petris Recall^{TM} Sigma module for a range of conditions (stress magnitudes [*Davidson et al*., 2012], reservoir temperature, and rock properties [*Siratovich et al*., 2012]). Figure 8 shows an example of DITF initiation tendency for well RK30L1 for a depth where a DITF is observed (~2381 mRF). A range of S_{Hmax} magnitudes ($S_{hmin} \leq S_{Hmax} \leq S_v$) is explored (as this is the least constrained stress magnitude), pore pressure (P_p) is set to hydrostatic (as an upper limit for this geothermal field), and values of ΔT and T are set at measurements that most limit tensile crack formation (i.e., lowest ΔT and highest T) recorded for the wells and formations concerned. For S_{Hmax} values equal or close to S_{hmin}, initiation tendency of DITFs is unlikely for the given well orientation, implying that for the Rotokawa Geothermal Field (at least in this location) S_{Hmax} must be greater than S_{hmin} by a minimum factor of ~40%. High values of ΔT (100–290°C) in the reservoir produce a more tensile stress concentration around the borehole explaining the lack of observed borehole breakouts on BHTV logs.

5.5. DITF Morphology

The occurrence of borehole axial DITF morphologies in these deviated wells is unexpected as previous study indicates that they should have en echelon morphologies [*Aadnøy and Bell*, 1998; *Peška and Zoback*, 1995]. This is reiterated by modeling (using the Petris^{TM} Sigma module) the expected DITF orientations, at the depths they occur in each well, using the appropriate borehole orientation, reservoir properties (Poisson's ratio, coefficient of internal friction, tensile strength, unconfined compressive strength, Young's modulus, and coefficient of thermal expansion), and stress parameter (orientations, magnitudes, and pore pressures). For all cases modeled in the three study wells, en echelon DITF morphologies are expected. The observed axial morphologies may be due to deviation of the σ_1 (S_v) to align with the borehole axes, allowing axial DITFs to develop. As all three study wells are deviated in different directions, this would require the σ_1 orientation to vary across the geothermal field. Localized stress perturbations, caused by slip on fracture planes, may cause rotation of the stress field, potentially aligning σ_1 to the borehole axis. A similar phenomenon (though in reverse) is noted from the observation of DITFs on the deep KTB well BHTV images in Germany [*Brudy et al*., 1997]. Perturbations of the in situ horizontal stress field, resulting from slip on fracture planes, caused the formation of en echelon DITFs in the vertical KTB well. As axial morphologies are observed along the entirety of the BHTV logged intervals in the Rotokawa study wells, the majority of observed structures would need to be active to perturb the stress field orientation along the entire well length.

5.6. Form and Origins of In Situ Stress Field Orientation Heterogeneity

The observed in situ horizontal stress field orientations are consistent with the extensional setting of the TVZ, stress orientations determined from earthquake focal mechanisms [*Hurst et al*., 2002; *Townend et al*., 2012;

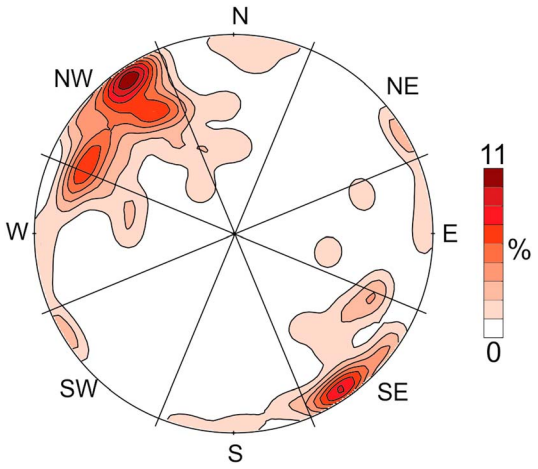

Figure 9. Contoured, lower hemisphere stereonet of pole to planes of fractures over which DITF orientation display a rotation of >10°. Stereonets contoured using Fisher Distribution with color scales representing percentages.

Seebeck et al., 2014], and in situ horizontal stress field orientations reported from other TVZ geothermal fields in vertical and subvertical wells [*McLean and McNamara*, 2011; *Wallis et al*., 2012; *Massiot et al*., 2013].

As with the observed structural patterns, in situ horizontal stress field orientations are not homogeneous across the field or with depth. A difference of ~19°–24° in the mean S_{Hmax} direction (Table 5) between well RK18L2 and wells RK30L1 and RK32 may imply a field-scale perturbation of the stress field between these wells, or a compartmentalization of the field into areas of different stress orientation regimes. However, this variation in mean S_{Hmax} falls within the standard deviations (Table 5) and may be statistical. Further stress field perturbations are noted on the well scale. In wells RK30L1 and RK32 S_{Hmax}, orientations show large rotations (greater than 1 standard deviation from the mean) over numerous <10 m depth intervals. Well RK18L2 contains a bimodal S_{Hmax} direction pattern related to depth, produced by a horizontal stress field rotation of ~32°.

These perturbations in the in situ horizontal stress field orientation result from geological effects, such as variation in the mechanical behavior (e.g., compressive strength and Young's modulus) within or between rock types, or slip on a fault or fracture plane. In the three study wells there are a number of correlations between in situ stress field rotations and lithological variation. The large in situ horizontal stress field rotation in well RK18L2 (Figure 5) occurs between ~1390 and 1510 mRF. This interval contains two lithological boundaries: andesite to the underlying volcaniclastics of the Tahorakuri Formation (~1380 mRF) and back into underlying andesite (~1455 mRF). Either of these lithological transitions, presuming a significant contrast between their mechanical properties, may be responsible for the observed perturbation of the stress field. Further correlation of in situ horizontal stress field rotations and transition into a potentially mechanically stronger lithology occur at ~1700 mRF in well RK32 (change from the sedimentary Waikora Formation to andesite), and at ~1625 mRF in well RK30L1 (within 5 m of the lithological transition from the Waikora Formation to the Tahorakuri Formation).

Similar in situ stress field rotations, at the scales observed here, can be found in other geothermal fields where they are attributed to slip on faults or fractures [*Davatzes and Hickman*, 2010b; *Blake*, 2013]. Activity on the PFF may have perturbed the in situ stress field enough to explain the difference between S_{Hmax} orientations observed in well RK18L2 and those in wells RK32 and RK30L1. In addition, it may also explain the depth-related in situ stress field rotation observed in well RK18L2 (~1390–1510 mRF). Azimuthal variation of DITFs occurring either side of an identified fracture are observed on BHTV logs from all three study wells (~44% of total DITFs and single DITFs observed). This indicates some of the depth-related in situ stress field orientation heterogeneity is due to recent slip on these fractures, which have a dominant NE-SW strike dipping both NW and SE, which is consistent with the regional strike of active faults in the rift (Figure 9).

5.7. Structural Permeability

Permeability in a geothermal reservoir is a composite of many factors including intrinsic permeability, structure, stress and reservoir mechanics [*Davatzes and Hickman*, 2010a], chemical effects such as mineral deposition and precipitation [*Dempsey et al*., 2012; *Dobson et al*., 2003], and self-propping fractures facilitated by fracture roughness [*Brown*, 1987] or mineral bridging [*Laubach et al*., 2004]. To fully comprehend geothermal reservoir permeability, a completely coupled thermochemical-mechanical approach must be taken. The work presented here focuses on the structural/mechanical aspect of permeability in the Rotokawa Geothermal Reservoir.

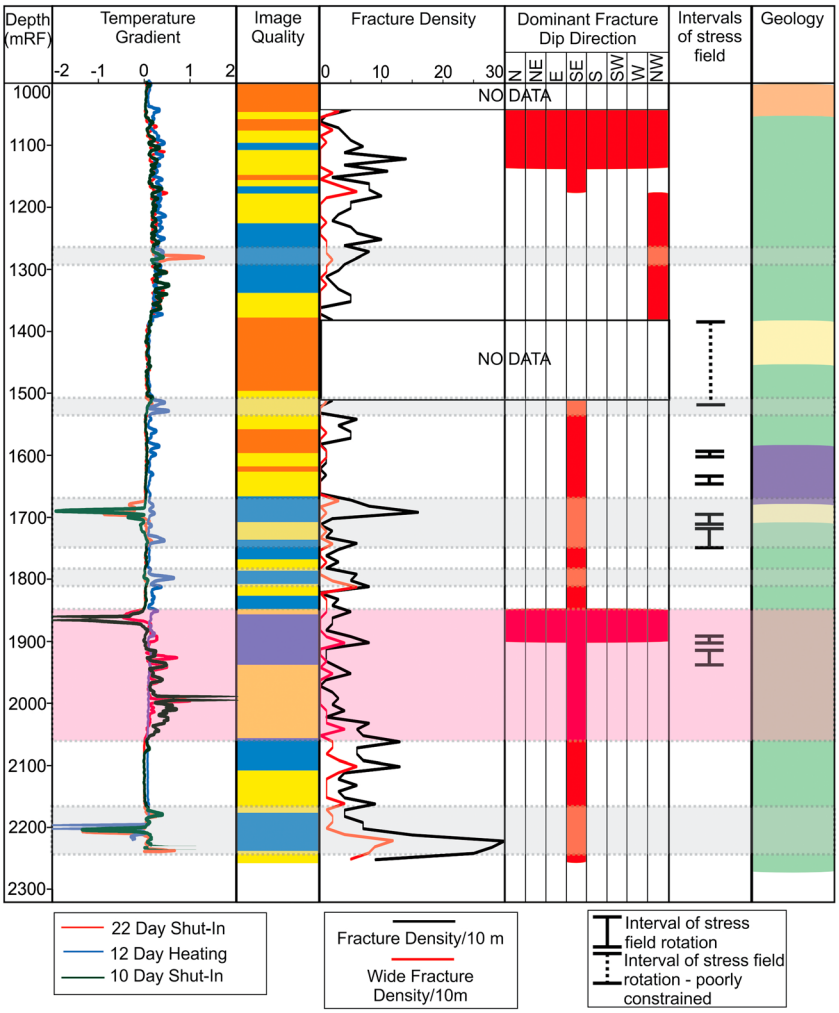

Figure 10. Compilation of temperature gradient, acoustic image quality, fracture density, dominant fracture dip direction, in situ stress field rotation, and lithology logs (Lithology color coded to key shown for lithology in Figure 2.) from well RK18L2. Permeable intervals are projected over these logs in green. Grey shaded zones are minor permeable zones, pink shaded zone indicates major permeable zone.

Permeable zones for the three study wells were defined using modeled feed zone data and detailed temperature gradient profiles. The depth intervals and quantitative magnitudes of the main feed zones are interpreted from pressure, temperature, spinner logs using wellbore modeling techniques, while taking into account logs collected under several different operating conditions. Temperature gradients provide depths of wellbore flows but only a qualitative understanding of the magnitude. A gradient was calculated for each available temperature log because they vary depending on well operation conditions (i.e., shut, injection or production, and the flow rates in the well) and how close the well is to equilibrium (i.e., well heating after drilling). Integration of the various log data allows a complete characterization of a well's permeability profile, which cannot be observed from a single log at one given set of well operation conditions or flow/injection rates.

Permeable zones from wells RK18L2, RK30L1, and RK32 are projected onto structure and stress data acquired from the BHTV logs of these wells (e.g., Figure 10, well RK18L2). These correlations indicate that all but one permeable zone contains wide aperture fractures and approximately two thirds contain high fracture densities. In situ stress field rotations (>1 standard deviation of the mean and occurring within a 10 m interval) are observed in 50% of the permeable zones. Figure 11 shows a dominant SE dip direction for fractures observed within permeable zones (28% of all fractures observed from BHTV logs for all three wells)

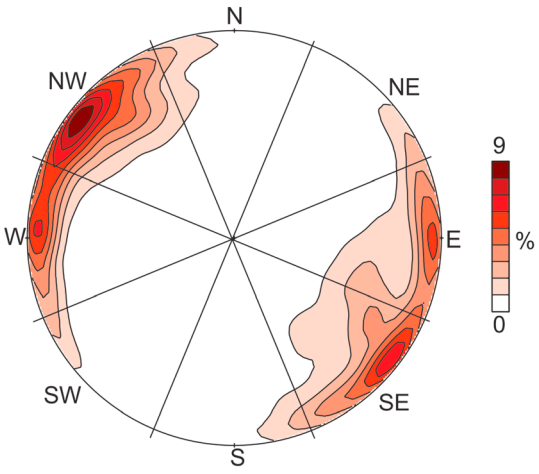

Figure 11. Contoured, lower hemisphere stereonet of poles to planes of fractures contained within permeable zones of the three study wells. Stereonets contoured using Fisher Distribution with color scales representing percentages.

with subordinate populations dipping NW (23%), W (12%), and E (14%). This confirms that structure plays a role in permeability in the Rotokawa Geothermal Field and that those orientations most likely to be flowing are those that parallel the orientations of large faults in the field and fault orientations of the Taupo rift.

A significant number of fractures observed from BHTV logs do not fall within permeable zones including two thirds of the wide aperture fractures and 60% of high fracture density peaks. These fractures have similar character and orientation to those within permeable zones yet are somehow fundamentally different in that they are currently not channeling fluid flow in the reservoir. There are a number of possibilities as to why this is the case. As discussed, the nature of a low acoustic amplitude fracture in a geothermal environment is yet to be fully understood. It is entirely possible that these low-amplitude fractures outside of permeable zones are sealed with a hydrothermal mineral that significantly attenuates the acoustic wave (e.g., hydrothermal clays such as chlorite). Additionally, BHTV logs only image fractures as they appear at the surface of the borehole. It may be the case that a sealed fracture has "opened" at the borehole wall due to drilling or localized unloading thus appearing as a discordant, low-amplitude feature, whereas in reality it is actually sealed a short distance into the formation. These fractures may indeed be open but have poor connectivity away from the borehole and thus are poor fluid flow pathways. Given the heterogeneity of the in situ horizontal stress field orientations throughout the Rotokawa Geothermal Field, structures optimally oriented for reactivation in some areas, and thus allow fluid flow, may not be in other areas and thus remain inactive and sealed to fluid flow. Finally, the lack of information on fracture length and connectivity hinders assessment of fracture fluid conductivity at the reservoir scale.

6. Conclusions

Fracture orientations, densities and apertures in the Rotokawa Geothermal Field are heterogeneous at a variety of scales. A dominant NE-SW fracture strike trend persists across the field related to proximity to larger-scale graben faults. Depth-related switches from dominant dip directions within individual well data sets are interpreted here to be signals of antithetic faulting expected from an extensional environment. Variation in fracture densities are thought to be linked to fault damage zones at least within the andesites of the Rotokawa Field, where there is enough confidence in the density variation being natural and not related to image quality degradation.

Stress orientation measurements were made predominantly from DITFs in the study wells. Their abundance over other induced borehole features results from the interplay between the borehole fluid and formation temperatures and the stress conditions around the borehole during drilling. Field-scale heterogeneity, taking the form of a rotation in the S_{Hmax} between well RK18L2 and wells RK30L1 and RK32, is attributed to recent activity on the PFF fault in the region of well RK18L2, which perturbed the in situ stress field orientations. Well-scale rotations in the in situ horizontal stress field are mainly observed to occur over a single fracture or group of fractures, with predominantly NE-SW strike orientations and are thus caused by recent localized slip on these features. The occurrence of fracture slip may also be evidenced by the observed preference of DITFs to have a borehole axial morphology. This heterogeneity in in situ horizontal stress field orientation is important to fluid flow considerations as it will impact which structures across the field are critically stressed and thus potential fluid flow pathways.

Correlation of permeable zones from study wells to data acquired from BHTV logs show that most permeable zones contain wide aperture fractures and, to a slightly lesser extent, high fracture densities. It is also noted that some zones of significant in situ horizontal stress field rotation correlate with permeable zones. These results indicate that fractures, and recent activity on those fractures, influences fluid flow in the Rotokawa Geothermal Field. Fractures identified as potentially open to fluid flow have a dominant NE-SW strike trend with NW dip directions. However, structures similar to those identified in permeable zones occur elsewhere in the study wells. Thus, while fracturing may not be a reliable means of predicting specific occurrence of permeability within a well, BHTV data suggest that it has a significant role in fluid flow control and potentially introduces an element of anisotropy to fluid flow, in that structures identified within permeable zones have a preferred NE-SW strike.

Acknowledgments

Acknowledgements go to the Geothermal Resources of New Zealand research program at GNS Science for funding for this work, and the Rotokawa Joint Venture Ltd. (Mighty River Power Ltd. and Tauhara North No. 2 Trust) for allowing release of data and for providing comment. Recall™ software provided by Halliburton, Landmark Software and Services. The authors thank A. Nicol and M. Lawrence for useful comments. Data used in this work are proprietary to Rotokawa Joint Venture Ltd and GNS Science. Authors may be contacted to request access to data.

References

Aadnøy, B. S., and J. S. Bell (1998), Classification of drilling-induced fractures and their relationship to in-situ stress directions, *Log Analyst*, *39*, 27–42.

Alcaraz, S. A., M. S. Rattenbury, M. D. Rosenberg, S. Soengkono, G. Bignall, and H. van Moerkerk (2011), 3D visualisation model of the Taupo Volcanic Zone basement, in *NZ Geothermal Workshop*, *Proc. N. Z. Geotherm. Workshop*, vol. 33, p. 8, Workshop Programme, Auckland.

Anderson, E. M. (1905), The dynamics of faulting, *Trans. Edinburgh Geol. Soc.*, *8*, 393–402, doi:10.1144/transed.8.3.387.

Arehart, G., B. W. Christenson, C. P. Wood, K. A. Foland, and P. R. L. Browne (2002), Timing of volcanic, plutonic and geothermal activity at Ngatamariki, New Zealand, *J. Volcanol. Geotherm. Res.*, *116*, 201–214, doi:10.1016/S0377-0273(01)00315-8.

Asanuma, H., N. Soma, H. Kaieda, Y. Kumano, T. Izumi, K. Tezuka, H. Niitsuma, and D. Wyborn (2005), Microseismic monitoring of hydraulic stimulation at the Australian HDR Project in Cooper Basin, Proceedings World Geothermal Congress 2005, Int. Geotherm. Assoc., Antalya, Turkey, 24–29 April.

Bannister, S., S. Sherburn, T. Powell, and D. Bowyer (2008), Microearthquakes at the Rotokawa Geothermal Field, New Zealand, *GRC Trans.*, *32*, 259–264.

Barton, C. A., S. H. Hickman, R. Morin, M. D. Zoback, and D. Benoit (1998), Reservoir-scale fracture permeability in the Dixie Valley, Nevada, Geothermal Field, Proceedings Twenty-Third Workshop on Geothermal Reservoir Engineering, 1998, 299-306, Stanford Univ., Stanford, Calif.

Barton, C. A., D. Moos, L. Hartley, S. Baxter, L. Foulquier, H. Holl, and R. Hogarth (2013), Geomechanically coupled simulation of flow in fractured reservoirs, Proceedings, Thirty-Eighth Workshop on Geothermal Reservoir Engineering, Stanford Univ., Stanford, Calif., February 11–13, 2013 SGP-TR-198.

Begg, J. G., and V. Mouslopoulou (2010), Analysis of late Holocene faulting within an active rift using lidar, Taupo Rift, New Zealand, *J. Volcanol. Geotherm. Res.*, *190*, 152–167, doi:10.1016/j.jvolgeores.2009.06.001.

Bertani, R. (2012), Geothermal power generation in the world 2005–2010 update report, *Geothermics*, *41*, 1–29, doi:10.1016/j.geothermics.2011.10.001.

Bibby, H. M., T. Caldwell, F. Davey, and T. Webb (1995), Geophysical evidence on the structure of the Taupo Volcanic Zone and its hydrothermal circulation, *J. Volcanol. Geotherm. Res.*, *68*, 29–58, doi:10.1016/0377-0273(95)00007-H.

Bignall, G., A. Rae, and M. D. Rosenberg (2010), Rationale for targeting fault versus formation-hosted permeability in high-temperature geothermal systems of the Taupo Volcanic Zone, New Zealand, in *Proceedings of the World Geothermal Congress 2010*, p. 7, Int. Geotherm. Assoc., Bali, Indonesia.

Blackwell, D. D., P. T. Negraru, and M. C. Richards (2007), Assessment of the enhanced geothermal system resource base of the United States, *Nat. Resour. Res.*, *15*, 283–308, doi:10.1007/s11053-007-9028-7.

Blake, K. (2013), Stress analysis for boreholes on Department of Defence lands in the western United States: A study in stress heterogeneity, Proceedings, Thirty-Eighth Workshop on Geothermal Reservoir Engineering, Stanford Univ., Stanford, Calif.

Blake, K., and N. C. Davatzes (2011), Crustal stress heterogeneity in the vicinity of Coso Geothermal Field, CA, Proceedings, Thirty-Sixth Workshop on Geothermal Reservoir Engineering, p. 11, Coso, Calif.

Brace, W. F. (1980), Permeability of crystalline and argillaceous rocks, *Int. J. Rock Mech. Min. Sci. Geomech. Abstr.*, *17*, 241–251, doi:10.1016/0148-9062(80)90807-4.

Brown, S. R. (1987), Fluid flow through rock joints: The effect of surface roughness, *J. Geophys. Res.*, *92*, 1337–1347, doi:10.1029/JB092iB02p01337.

Browne, P. R. L., I. J. Graham, R. J. Parker, and C. P. Wood (1992), Subsurface andesite lavas and plutonic rocks in the Rotokawa and Ngatamariki geothermal systems, Taupo Volcanic Zone, New Zealand, *J. Volcanol. Geotherm. Res.*, *51*, 199–215, doi:10.1016/0377-0273(92)90123-U.

Brudy, M., M. D. Zoback, K. Fuchs, F. Rummel, and J. Baumgärtner (1997), Estimation of the complete stress tensor to 8 km depth in the KTB scientific drill holes: Implications for crustal strength, *J. Geophys. Res.*, *102*, 18,453–18,475, doi:10.1029/96JB02942.

Bruno, M. S., and D. F. Winterstein (1994), Some influences of stratigraphy and structure on reservoir stress orientation, *Geophysics*, *59*, 954–962, doi:10.1190/1.1443655.

Budkewitsch, P., and P.-Y. Robin (1994), Modelling the evolution of columnar joints, *J. Volcanol. Geotherm. Res.*, *59*, 219–239, doi:10.1016/0377-0273(94)90092-2.

Cheung, P. S. (1999), Microresistivty and ultrasonic imagers: Tool operations and processing principles with reference to commonly encountered image artefacts, in *Borehole Imaging: Applications and Case Histories*, edited by M. A. Lovell, G. Williamson, and P. K. Harvey, *Geol. Soc. London Spec. Publ.*, *159*, 45–57, doi:10.1144/GSL.SP.1999.159.01.02.

Co, C. K. D. (2012), Characterization of geothermal feedzones and interwell connectivity, MS thesis, School of Earth Sciences, Stanford Univ., Stanford, Calif.

Cole, J. W., and K. D. Spinks (2009), Caldera volcanism and rift structure in the Taupo Volcanic Zone, New Zealand, *Geol. Soc. London Spec. Publ.*, *327*, 9–29, doi:10.1144/SP327.2.

Collar, R. J., and P. R. L. Browne (1985), Hydrothermal eruptions at the Rotokawa Geothermal Field, Taupo Volcanic Zone, Proceedings, Seventh New Zealand Geothermal Workshop, Taupo Volcanic Zone, Rotokawa, New Zealand.

Davatzes, N. C., and S. Hickman (2005), Comparison of acoustic and electrical image logs from the Coso geothermal field, CA, Proceedings, Thirtieth Workshop on Geothermal Reservoir Engineering, Stanford Univ., Stanford, Calif.

Davatzes, N. C., and S. H. Hickman (2010a), Stress, fracture, and fluid-flow analysis using acoustic and electrical image logs in hot fractured granites of the Coso Geothermal Field, California, U.S.A., in *Dipmeter and Borehole Image Log Technology*, *AAPG Mem.*, vol. 92, edited by M. Pöppelreiter, C. García-Carballido, and M. Kraaijveld, pp. 259–293, Am. Assoc. Petroleum Geolog., doi:10.1306/13181288M923134.

Davatzes, N. C., and S. H. Hickman (2010b), The feedback between stress, faulting, and fluid flow: Lessons from the Coso Geothermal Field, CA, U.S.A., Proceedings, World Geothermal Congress 2010, p. 15, Int. Geotherm. Assoc., Bali, Indonesia, 25–29 April.

Davidson, J., P. Siratovich, I. C. Wallis, D. Graveley, and D. D. McNamara (2012), Quantifying the stress distribution at the Rotokawa Geothermal Field, New Zealand, Proceedings of 34th New Zealand Geothermal Workshop, 19–21 November, Auckland Univ., Auckland, New Zealand.

DeGraff, J. M., and A. Aydin (1987), Surface morphology of columnar joints and its significance to mechanics and direction of joint growth, *Geol. Soc. Am. Bull.*, *99*, 605–617, doi:10.1130/0016-7606(1987)99<605:SMOCJA>2.0.CO;2.

Dempsey, D., J. Rowland, and R. Archer (2012), Modelling geothermal fluid flow and silica deposition along an active fault, Proceedings, 37th Workshop on Geothermal Reservoir Engineering, Stanford Univ., Stanford, Calif.

Dezayes, C., A. Genter, and B. T. Valley (2010), Structure of the low permeable naturally fractured geothermal reservoir at Soultz, *C. R. Geosci.*, *342*, 517–530, doi:10.1016/j.crte.2009.10.002.

Dobson, P. F., T. J. Kneafsey, E. L. Sonnenthal, N. Spycher, and J. A. Apps (2003), Experimental and numerical simulation of dissolution and precipitation: Implications for fracture sealing at Yucca Mountain, Nevada, *J. Contam. Hydrol.*, *62*, 459–476, doi:10.1016/S0169-7722(02)00155-9.

García-Carballido, C., J. Boon, and N. Tso (2010), Data management and quality control of dipmeter and borehole image log data, in *Dipmeter and Borehole Image Log Technology*, *AAPG Mem.*, vol. 92, edited by M. Pöppelreiter, C. García-Carballido, and M. Kraaijveld, pp. 259–293, Am. Assoc. Petrol. Geol., doi:10.1306/13181288M923134.

Grindley, G. W., P. R. L. Browne, and M. Gardner (1985), Surface and subsurface geology, Rotokawa Geothermal Field, Ministry of Works and Development Report to the Ministry of Energy, New Zealand.

Grohmann, C. H., and G. A. C. Campanha (2010), OpenStereo: Open source, cross-platform software for structural geology analysis, Abstract IN31C-06 presented at 2010 Fall Meeting, AGU, San Francisco, Calif., 13–17 Dec.

Gudmundsson, A., I. Fjeldskaar, and S. L. Brenner (2002), Propagation pathways and fluid transport of hydrofractures in jointed and layered rocks in geothermal fields, *J. Volcanol. Geotherm. Res.*, *116*, 257–278, doi:10.1016/S0377-0273(02)00225-1.

Heise, W., T. G. Caldwell, H. M. Bibby, and S. C. Bannister (2008), Three-dimensional modelling of magnetotelluric data from the Rotokawa geothermal field, Taupo Volcanic Zone, New Zealand, *Geophys. J. Int.*, *173*, 740–750, doi:10.1111/j.1365-246X.2008.03737.x.

Hetényi, G., B. Taisne, F. Garel, É. Médard, S. Bosshard, and H. B. Mattsson (2012), Scales of columnar jointing in igneous rocks: Field measurements and controlling factors, *Bull. Volcanol.*, *74*, 457–482, doi:10.1007/s00445-011-0534-4.

Hurst, A. W., H. M. Bibby, and R. R. Robinson (2002), Earthquake focal mechanisms in the central Taupo Volcanic Zone and their relation to faulting and deformation, *N. Z. J. Geol. Geophys.*, *45*, 527–536, doi:10.1080/00288306.2002.9514989.

Hurst, T., S. Bannister, R. Robinson, and B. Scott (2008), Characteristics of three recent earthquake sequences in the Taupo Volcanic Zone, New Zealand, *Tectonophysics*, *452*, 17–28, doi:10.1016/j.tecto.2008.01.017.

Ito, T., and M. D. Zoback (2000), Fracture permeability and in situ stress to 7 km depth in the KTB scientific drillhole, *Geophys. Res. Lett.*, *27*, 1045–1048, doi:10.1029/1999GL011068.

Johnson, R. B. (1961), Patterns and origin of radial dike swarms associated with West Spanish Peak and Dike Mountain, south-central Colorado, *Geol. Soc. Am. Bull.*, *72*, 579–589, doi:10.1130/0016-7606(1961)72[579:PAOORD]2.0.CO;2.

Krupp, R. E., and T. M. Seward (1987), The Rotokawa geothermal system, New Zealand: An active epithermal gold-depositing environment, *Econ. Geol.*, *82*, 1109–1129, doi:10.2113/gsecongeo.82.5.1109.

Lamarche, G., P. M. Barnes, and J. M. Bull (2006), Faulting and extension rates over the last 20,000 years in the offshore Whakatane Graben, New Zealand continental shelf, *Tectonophysics*, *25*, 1–24, doi:10.1029/2005TC001886.

Laubach, S. E., J. E. Olson, and J. F. W. Gale (2004), Are open fractures necessarily aligned with maximum horizontal stress?, *Earth Planet. Sci. Lett.*, *222*, 191–195, doi:10.1016/j.epsl.2004.02.019.

Lee, C.-C., C.-H. Lee, H.-F. Yeh, and H.-I. Lin (2011), Modeling spatial fracture density as a control on fluid flow in fractured rock, *Environ. Earth Sci.*, *63*, 1199–1211, doi:10.1007/s12665-010-0794-x.

Legarth, B., E. Huenges, and G. Zimmerman (2005), Hydraulic fracturing in a sedimentary geothermal reservoir: Results and implications, *Int. J. Rock Mech. Min. Sci.*, *42*, 1028–1041, doi:10.1016/j.ijrmms.2005.05.014.

Lin, W., E.-C. Yeh, J.-H. Hung, B. Haimson, and T. Hirono (2010), Localized rotation of principal stress around faults and fractures determined from borehole breakouts in hole B of the Taiwan Chelungpu-fault Drilling Project (TCDP), *Tectonophysics*, *482*, 82–91, doi:10.1016/j.tecto.2009.06.020.

Litchfield, N. J., et al. (2014), A model of active faulting in New Zealand, *N. Z. J. Geol. Geophys.*, *57*, 32–56, doi:10.1080/00288306.2013.854256.

Lofts, J. C., and L. T. Bourke (1999), The recognition of artefacts from acoustic and resistivity borehole imaging devices, *Geol. Soc. London Spec. Publ.*, *159*, 59–76, doi:10.1144/GSL.SP.1999.159.01.03.

Long, J. C. S., and P. A. Witherspoon (1985), The relationship of the degree of interconnection to permeability in fracture networks, *J. Geophys. Res.*, *90*, 3087–3098, doi:10.1029/JB090iB04p03087.

Martin, C. D., and N. A. Chandler (1993), Stress heterogeneity and geological structures, *Int. J. Rock Mech. Min. Sci. Geomech. Abstr.*, *30*, 993–999, doi:10.1016/0148-9062(93)90059-M.

Massiot, C., D. D. McNamara, B. Lewis, L. Price, and G. Bignall (2012), Statistical corrections of fracture sampling bias in boreholes from acoustic televiewer logs, Proceedings 34th New Zealand Geothermal Workshop, Auckland Univ., Auckland.

Massiot, C., D. D. McNamara, and B. Lewis (2013), Interpretative review of the acoustic borehole image logs acquired to date in the Wairakei-Tauhara Geothermal Field, *GNS Science Report 2013/04*, GNS Science, New Zealand.

Massiot, C., D. D. McNamara, and B. Lewis (2015), Processing and analysis of high temperature geothermal acoustic borehole image logs, New Zealand, *Geothermics*, *53*, 190–201, doi:10.1016/j.geothermics.2014.05.010.

McLean, K., and D. D. McNamara (2011), Fractures interpreted from acoustic formation imaging technology: Correlation to permeability, Proceedings, Thirty-Sixth Workshop on Geothermal Reservoir Engineering, Stanford Univ., Stanford, Calif.

McNamara, D. D., C. Massiot, and B. Lewis (2013), A structural review of the Wairakei-Tauhara Geothermal Field, *GNS Science Report 2013/03*, GNS Science, New Zealand.

McNamara, D. D., D. Faulkner, and E. McCarney (2014), Rock properties of greywacke basement hosting geothermal reservoirs, New Zealand: Preliminary results, Proceedings, Thirty-Ninth Workshop on Geothermal Reservoir Engineering, Stanford Univ., Stanford, Calif.

Milicich, S. D., C. J. N. Wilson, G. Bignall, B. Pezaro, and C. Bardsley (2013), Reconstructing the geological and structural history of an active geothermal field: A case study from New Zealand, *J. Volcanol. Geotherm. Res.*, *262*, 7–24, doi:10.1016/j.jvolgeores.2013.06.004.

Nicol, A., J. Walsh, K. Berryman, and P. Villamor (2006), Interdependence of fault displacement rates and paleoearthquakes in an active rift, *Geology*, *34*, 865–868, doi:10.1130/G22335.1.

Nie, X., C. Zou, L. Pan, Z. Huang, and D. Liu (2013), Fracture analysis and determination of in-situ stress direction from resistivity and acoustic image logs and core data in the Wenchuan Earthquake Fault Scientific Drilling Borehole-2 (50 ~ 1370 m), *Tectonophysics*, *593*, 161–171, doi:10.1016/j.tecto.2013.03.005.

Parkinson, D. N., R. J. Dixon, and E. J. Jolley (1999), Contributions of acoustic imaging to the development of the Bruce Field, Northern North Sea, *Geol. Soc. London Spec. Publ.*, *159*, 259–270, doi:10.1144/GSL.SP.1999.159.01.14.

Peška, P., and M. D. Zoback (1995), Compressive and tensile failure of inclined well bores and determination of in situ stress and rock strength, *J. Geophys. Res.*, *100*, 12,791–12,811, doi:10.1029/95JB00319.

Philipp, S. L., F. Afşar, and A. Gusmundsson (2013), Effects of mechanical layering on hydrofracture emplacement and fluid transport in reservoirs, *Front. Earth Sci.*, *1*, 1–19, doi:10.3389/feart.2013.00004.

Quinao, J. J., and L. Sirad-Azwar (2012), Correlation of reservoir monitoring and continuous production data to interpret unexpected well behaviour in Rotokawa, New Zealand Geothermal Workshop 2012 Proceedings, 19–21 November 2012, Auckland Univ., Auckland, New Zealand.

Quinao, J., L. Sirad-Azwar, J. Clearwater, V. Hoepfinger, M. Le Brun, and C. Bardsley (2013), Analyses and modelling of reservoir pressure changes to interpret the Rotokawa Geothermal Field response to Nga Awa Purua Power Station operation, Proceedings, Thirty-Eighth Workshop on Geothermal Reservoir Engineering, Stanford Univ., Stanford Geothermal Program, Stanford, Calif.

Rae, A. (2007), Rotokawa Geology and Geophysics, *GNS Science Consultancy Report 2007/83*, GNS Science, New Zealand.

Rae, A. J., J. O'Brien, E. Ramirez, and G. Bignall (2011), The application of chlorite geothermometry to hydrothermally altered Rotokawa Andesite, Rotokawa Geothermal Field, in *NZ Geothermal Workshop*, *Proc. N. Z. Geotherm. Workshop*, vol. 33, p. 8, Workshop Programme, Auckland.

Risk, G. F. (2000), Electrical resistivity of the Rotokawa Geothermal Field, New Zealand, Proceedings, 22nd New Zealand Geothermal Workshop, Taupo Volcanic Zone, Rotokawa, New Zealand.

Rosenberg, M. D., G. Bignall, and A. J. Rae (2009), The geological framework of the Wairakei-Tauhara Geothermal System, New Zealand, *Geothermics*, *38*, 72–84, doi:10.1016/j.geothermics.2009.01.001.

Rowland, J. V., and R. H. Sibson (2004), Structural controls on hydrothermal flow in a segmented rift system, Taupo Volcanic Zone, New Zealand, *Geofluids*, *4*, 259–283, doi:10.1111/j.1468-8123.2004.00091.x.

Rowland, J. V., and S. F. Simmons (2012), Hydrologic, magmatic, and tectonic controls on hydrothermal flow, Taupo Volcanic Zone, New Zealand: Implications for the formation of epithermal vein deposits, *Econ. Geol.*, *107*, 427–457, doi:10.2113/econgeo.107.3.427.

Sausse, J., M. Fourar, and A. Genter (2006), Permeability and alteration within the Soultz granite inferred from geophysical and flow log analysis, *Geothermics*, *35*, 544–560, doi:10.1016/j.geothermics.2006.07.003.

Schmitt, D. R., C. A. Currie, and L. Zhang (2012), Crustal stress determination from boreholes and rock cores: Fundamental principles, *Tectonophysics*, *580*, 1–26, doi:10.1016/j.tecto.2012.08.029.

Seebeck, H., A. Nicol, P. Villamor, J. Ristau, and J. Pettinga (2014), Structure and kinematics of the Taupo Rift, New Zealand, *Tectonics*, *33*, 1178–1199, doi:10.1002/2014TC003569.

Sewell, S. M., W. B. Cumming, L. Azwar, and C. Bardsley (2012), Integrated MT and natural state temperature interpretation for a conceptual model supporting reservoir numerical modelling and well targeting at the Rotokawa Geothermal Field, New Zealand, Proceedings, Thirty-Seventh Workshop on Geothermal Reservoir Engineering, Stanford Univ., Stanford, California, January 30–February 1, 2012, SGP-TR-194.

Sewell, S. M., W. Cumming, C. J. Bardsley, J. Winick, J. Quinao, I. C. Wallis, S. Sherburn, S. Bourguignon, and S. Bannister (2013), Interpretation of microearthquakes at the Rotokawa Geothermal Field, 2008 to 2012, 35th New Zealand Geothermal Workshop: 2013 Proceedings, 17–20 November 2013, Univ. Auckland, Auckland, New Zealand.

Sheridan, J. M., and S. H. Hickman (2004), In situ stress, fracture, and fluid flow analysis in Well 38C-9: An enhanced geothermal system in the Coso geothermal field, Proceedings, Twenty-Ninth Workshop on Geothermal Reservoir Engineering, Stanford Univ., Stanford, Calif., January 26–28, 2004 SGP-TR-175.

Siratovich, P. A., J. Davidson, M. Villeneuve, D. Graveley, B. Kennedy, J. Cole, L. Wyering, and L. Price (2012), Physical and mechanical properties of the Rotokawa Andesite from production wells RK 27_L2, RK 28 and RK 30, Proceedings of the New Zealand Geothermal Workshop, Univ. Auckland, Auckland, New Zealand.

Siratovich, P. A., M. J. Heap, M. C. Villenueve, J. W. Cole, and T. Reuschlé (2014), Physical property relationships of the Rotokawa Andesite, a significant geothermal reservoir rock in the Taupo Volcanic Zone, New Zealand, *Geotherm. Energy*, *2*, 1–31, doi:10.1186/s40517-014-0010-4.

Spörli, K. B., and J. V. Rowland (2006), 'Column on column' structures as indicators of lava/ice interaction, Ruapehu andesite volcano, New Zealand, *J. Volcanol. Geotherm. Res.*, *157*, 294–310, doi:10.1016/j.jvolgeores.2006.04.004.

Townend, J., S. Sherburn, R. Arnold, C. Boese, and L. Woods (2012), Three-dimensional variations in present-day tectonic stress along the Australia–Pacific plate boundary in New Zealand, *Earth Planet. Sci. Lett.*, *353–354*, 47–59, doi:10.1016/j.epsl.2012.08.003.

Valley, B. C. (2007), The relationship between natural fracturing and stress heterogeneities in deep-seated crystalline rocks at Soultz-sous-Forêts (France), PhD Thesis, Institute of Geology, Swiss Federal Institute of Technology (ETH) Zurich, Switzerland.

Valley, B., and K. F. Evans (2010), Stress heterogeneity in the granite of the Soultz EGS reservoir inferred from analysis of wellbore failure, paper presented at World Geothermal Congress, Int. Geotherm. Assoc., Bali, 25–29 April 2010.

Vigneresse, J. -L., B. Tikoff, and L. Améglio (1999), Modification of the regional stress field by magma intrusion and formation of tabular granitic plutons, *Tectonophysics*, *302*, 203–224, doi:10.1016/S0040-1951(98)00285-6.

Villamor, P., and K. R. Berryman (2001), A late Quaternary extension rate in the Taupo Volcanic Zone, New Zealand, derived from fault slip data, *N. Z. J. Geol. Geophys.*, *44*, 243–269, doi:10.1080/00288306.2001.9514937.

Wallace, L. M., J. Beavan, R. McCaffrey, and D. Darby (2004), Subduction zone coupling and tectonic block rotations in the North Island, New Zealand, *J. Geophys. Res.*, *109*, 1978–2012, doi:10.1029/2004JB003241.

Wallis, I. C., D. D. McNamara, J. Rowland, and C. Massiot (2012), The nature of fracture permeability in the basement greywacke at Kawerau Geothermal Field, New Zealand, Proceedings, Thirty-seventh Workshop on Geothermal Reservoir Engineering, Stanford Univ., Stanford, Calif., January 30–February 1, 2012.

Wallis, I. C., C. J. Bardsley, T. S. Powell, J. V. Rowland, and J. M. O'Brien (2013), A structural model for the Rotokawa Geothermal Field, New Zealand, 35th New Zealand Geothermal Workshop: 2013 Proceedings, Auckland Univ., Auckland, New Zealand.

Wileveau, Y., F. H. Cornet, J. Desroches, and P. Blumling (2007), Complete in situ stress determination in an argillite sedimentary formation, *Phys. Chem. Earth*, *32*, 866–878, doi:10.1016/j.pce.2006.03.018.

Wilson, C. J. N., B. F. Houghton, M. O. McWilliams, M. A. Lanphere, S. D. Weaver, and R. M. Briggs (1995), Volcanic and structural evolution of the Taupo Volcanic Zone, New Zealand: A review, *J. Volcanol. Geotherm. Res.*, *68*, 1–28, doi:10.1016/0377-0273(95)00006-G.

Wood, C. P., R. L. Brathwaite, and M. D. Rosenberg (2001), Basement structure, lithology and permeability at Kawerau and Ohaaki geothermal fields, New Zealand, *Geothermics*, *30*, 461–481, doi:10.1016/S0375-6505(01)00003-7.

Yoshioka, K., and J. Stimac (2010), Geologic and geomechanical reservoir simulation modeling of high pressure injection, West Salak, Indonesia, Proceedings of the World Geothermal Congress 2010, Int. Geotherm. Assoc., Bali, Indonesia, 25–29 April.

Zhang, A., and O. Stephansson (Eds.) (2010), *Stress Field of the Earth's Crust*, Springer, Dordrecht, Heidelberg, New York, doi:10.1007/978-1-4020-8444-7_5.

Zoback, M. D. (2010), *Reservoir Geomechanics*, Cambridge Univ. Press, Cambridge, U. K.

Zoback, M. D., C. A. Barton, M. Brudy, D. A. Castillo, T. Finkbeiner, B. R. Grollimund, D. B. Moos, P. Peška, C. D. Ward, and D. J. Wiprut (2003), Determination of stress orientation and magnitude in deep wells, *Int. J. Rock Mech. Min. Sci.*, *40*, 1049–1076, doi:10.1016/j.ijrmms.2003.07.001.